# Letters

## An Enhanced Quasi-CC Output Model of LCC-P Compensated Inductive-Power-Transfer Converters

Fei Xu, *Member, IEEE*, Yanjie Guo, *Member, IEEE*, and Xian Zhang, *Member, IEEE*

***Abstract*—It has been explored by current research that the inductor–capacitor–capacitor–parallel (LCC-P) compensated inductive-power-transfer (IPT) converters can achieve constant-current (CC) outputs. However, the CC output model is derived by fundamental-harmonic-analysis (FHA) in a frequency domain, which is not enough accurate to express the output current because the high-frequency current flowing into the rectifier is a discontinuous partial-sine waveform. In this letter, an enhanced-fundamental-harmonic-analysis (EFHA) of LCC-P-compensated IPT system is first proposed to accurately derive the output current model based on the steady-state operating waveforms in a time domain. Under our proposed EFHA, the derivation results show that the output current of LCC-P compensated IPT converters would degrade with the load resistance, and only quasi-CC output can be achieved within a certain load range. The proposed EFHA can be used to design LCC-P compensated IPT system to achieve a quasi-CC output to satisfy the charging requirements, otherwise, the accuracy of charging current and charging speed would be deteriorated with FHA. Both simulation and experiment results are presented to validate the accuracy of EFHA, which show good agreements with the theoretical analysis.**

***Index Terms*—Constant-current (CC), enhanced-fundamental-harmonic-analysis (EFHA), inductive-power-transfer (IPT), inductor–capacitor–capacitor–parallel (LCC-P).**

### I. Introduction

INDUCTIVE-POWER-TRANSFER (IPT) is widely used in wireless charging of electric vehicle because of its operation convenience and environment reliability [1]. A typical battery charging profile begins with constant-current (CC) mode until the threshold voltage is reached. To comply with the charging CC profile, an effective method to achieve CC output against the variations of equivalent resistance of battery in a simplest single-stage IPT converter (without extra dc–dc converters or adopting active rectifier) is based on the load independent current characteristics of different compensation typologies [2], [3].

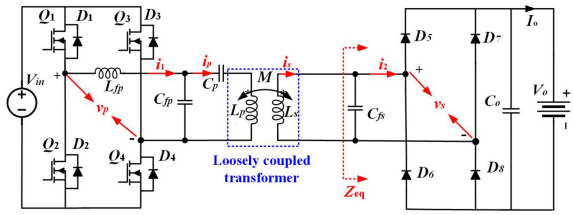


Fig. 1. Topology of LCC-P compensation of the IPT converter.

It is well known that the series–series (S-S) compensated IPT converter can achieve CC outputs, and the advantage of S-S compensation is that operating resonant frequency is independent of the coupling coefficient and the load [1], [2], [3]. However, since the output power would increase with the decrease of coupling coefficient, overcurrent problem would occur when there are misalignments [4]. In addition, it has been explored that the inductor–capacitor–capacitor–parallel (LCC-P) compensated IPT converter, as shown in Fig. 1, can also achieve CC outputs [5], [6]. Moreover, compared with the S-S compensated topology, the LCC-P compensation topology maintains the advantages of resonant frequency independent of the coupling coefficient and load, and it can easily avoid overcurrent problem and achieve open-load protection. Compared with LCC–LCC topology, the LCC-P compensation has a more compact receiver with fewer elements used on the receiver side, which can further decrease the size and weight of the receiver [6]. However, the derivations of LCC-P compensation with CC output are based on the fundamental-harmonic-analysis (FHA) in a frequency domain [5], [6]. The key problem is that the current flowing into the rectifier is a discontinuous partial-sine waveform, so using traditional FHA cannot obtain the mathematical output current model accurately. A time-domain analysis considering higher order harmonic components is proposed to accurate model the S-S compensated IPT system [7], [8]. However, the accurate analytical output models are not given and cannot be derived with the methods provided in [7], [8], and only numerical output results are solved with the help of MATLAB under a certain group system parameters. For other general system parameters, the complicated procedures need to be repeated again to get the

Manuscript received 12 July 2023; revised 7 August 2023 and 28 August 2023; accepted 11 September 2023. Date of publication 18 September 2023; date of current version 23 October 2023. This work was supported in part by the National Natural Science Foundation of China under Grants 51977147 and 52122701, in part by the Key Program of Natural Science Foundation of Tianjin under Grant 22JCZDJC00620, and in part by the Central Guiding Local Science and Technology Development Fund Projects under Grant 236Z5201G. *(Corresponding author: Yanjie Guo.)*

The authors are with the Department of Electrical Engineering and State Key Laboratory of Reliability and Intelligence of Electrical Equipment, Hebei University of Technology, Tianjin 300401, China (e-mail: feifly.xu@connect.polyu.hk; yjguofa@163.com; zhangxian@hebut.edu.cn).

Color versions of one or more figures in this article are available at https://doi.org/10.1109/TPEL.2023.3316225.

Digital Object Identifier 10.1109/TPEL.2023.3316225

output results, therefore, which is very difficult to be applied in practice for general design of IPT converters.

To tackle this problem, in this letter, an enhanced-fundamental-harmonic-analysis (EFHA) of LCC-P compensated IPT converter is first proposed to derive the output current model accurately based on the steady-state operating waveforms in a time domain. The equivalent circuit of the load side seen from the parallel capacitor is proposed innovatively to simplify the derivation process. Under our proposed EFHA, the results show that the output current would degrade with load resistance, and only quasi-CC output can be achieved in a certain load range. The quasi-CC means that the output current has a small tolerance error compared to the rated charging current. In practice, to provide rated charging currents with high precision, the proposed EFHA can be used to design the LCC-P compensated IPT system to achieve a quasi-CC output based on the variation range of equivalent resistance of battery, further meeting charging requirements. Moreover, the proposed EFHA maintains simplicity and elegance of FHA. Both simulation and experiment results are presented to validate the accuracy of EFHA, which are consistent with the theoretical analysis.

The contributions of this letter mainly include two aspects as follows. 1) We correct the traditional misconception of FHA that believes LCC-P can achieve load-independent CC output. In fact, the output current would decrease significantly with the increase of load resistance. 2) According to a novel equivalent circuit of LCC-P compensation IPT converters and the steady-state operating waveforms in time domain, an EFHA is first proposed to accurately derive the output current model.

## II. Quasi-CC Output With EFHA

Fig. 1 shows the topology of LCC-P compensated IPT system. For ease of reference, subscripts $p$ and $s$ denote parameters in the primary and secondary sides, respectively. The loosely coupled transformer has self-inductances $L_p$ and $L_s$ and mutual inductance $M$. The components of LCC compensation in the primary side include the series inductance $L_{fp}$, parallel capacitance $C_{fp}$, and series capacitance $C_p$. The parallel compensation in the secondary side includes the parallel capacitor $C_{fs}$.

The steady-state operating waveforms of a voltage-fed LCC-P compensated IPT converters with a capacitive filter are shown in Fig. 2. During the power transfer period ($\pi-\beta<\omega t<\pi$), the parallel capacitor voltage $v_{C_{fs}}$ is clamped by the output voltage $V_o$ and the resonant current $i_s$ supplies the load. Similarly, during the nonpower transfer period ($0<\omega t<\pi-\beta$), the entire $i_s$ engages in charging the parallel capacitor $C_{fs}$ and the filter capacitor $C_o$ feeds the load [9]. Because of this reason, the voltage of $v_{C_{fs}}$ is a clamped partial sinusoidal waveform, as shown in Fig. 2. In addition, due to nonlinear and nonsinusoidal characteristics of backend rectifier with a back capacitor filter, the current $i_2$ flowing into the rectifier is a discontinuous partial-sine waveform. To reduce the switching losses from the primary inverter, the conditions for ZVS should be maintained, which can be achieved by setting the operating frequency slightly higher than the system resonant frequency.

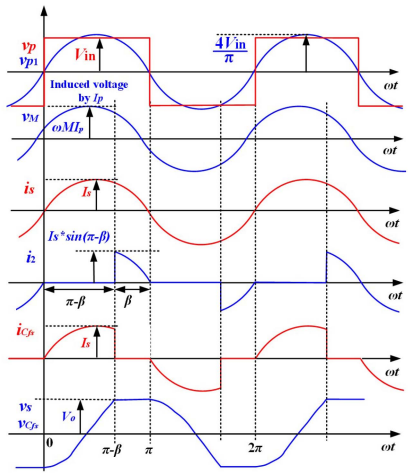


Fig. 2. Steady-state operating waveforms of a voltage-fed LCC-P IPT converters with a capacitive filter, as shown in Fig. 1.

The resonant current flowing through $C_{fs}$ is denoted as $i_{C_{fs}}$, according to Fig. 2, which can be expressed by

$$i_{C_{fs}}=\begin{cases} I_s\sin(\omega t), & 0<\omega t<\pi-\beta \\ 0, & \pi-\beta<\omega t<\pi \end{cases} \tag{1}$$

where $I_s$ is the peak value of $i_{C_{fs}}$, given by

$$I_s=\frac{2\omega C_{fs}V_o}{1+\cos\beta}. \tag{2}$$

The secondary diode conduction angle $\beta$ is

$$\beta=2\arctan\sqrt{\frac{\pi}{2\omega C_{fs}R_L}}. \tag{3}$$

According to (1) and (3), $v_{C_{fs}}$ can be calculated

$$v_{C_{fs}}(t)=\begin{cases} \frac{V_o(1-\cos\beta-2\cos\omega t)}{1+\cos\beta}, & 0<\omega t<\pi-\beta \\ V_o, & \pi-\beta<\omega t<\pi. \end{cases} \tag{4}$$

In addition, $v_{C_{fs}}(t)$ can also be expressed by

$$v_{C_{fs}}(t)=V_{C_{fs}}\sin(\omega t+\beta) \tag{5}$$

$$=V_{C_{fs}}[\cos\beta\sin\omega t+\sin\beta\cos\omega t] \tag{6}$$

$$=V_{C_{fs}\_d}\sin\omega t+V_{C_{fs}\_q}\cos\omega t \tag{7}$$

where $V_{C_{fs}\_d}$ and $V_{C_{fs}\_q}$ can be expressed as follows:

$$V_{C_{fs}\_d}=\frac{2V_o}{\pi}\frac{1-\cos\beta}{1+\cos\beta}\int_0^{\pi-\beta}\left(1-\frac{2\cos\omega t}{1-\cos\beta}\right)\times\cos\omega t d(\omega t)+\frac{2V_o}{\pi}\int_{\pi-\beta}^{\pi}\cos\omega t d(\omega t) \tag{8}$$

$$=\frac{2V_o(1-\cos\beta)}{\pi(1+\cos\beta)}\left(\sin\beta-\frac{\pi-\beta-\sin\beta\cos\beta}{1-\cos\beta}\right)-\frac{2V_O}{\pi}\sin\beta \tag{9}$$

$$=-\frac{2V_o(\pi-\beta+\sin\beta\cos\beta)}{\pi(1+\cos\beta)}, \text{and} \tag{10}$$

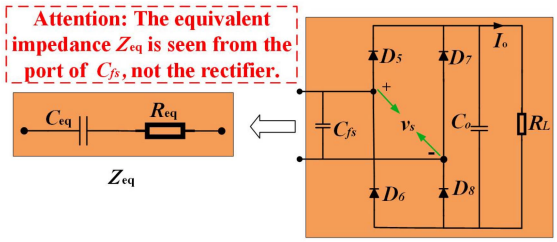


Fig. 3. Equivalent circuit of the backend rectifier with a back capacitor filter and load resistance seen from front parallel capacitance $C_{\rm fs}$.

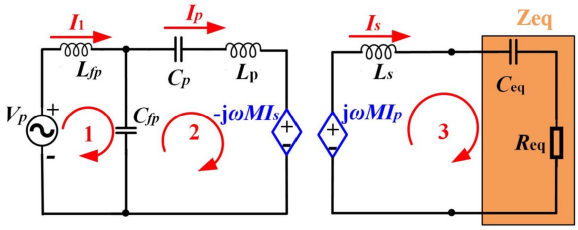


Fig. 4. Equivalent circuit of the LCC-P compensated IPT converters with $Z_{\rm eq}$.

$$V_{C_{fs}q} = \frac{2V_o}{\pi}\frac{1-\cos\beta}{1+\cos\beta}\int_0^{\pi-\beta}\left(1-\frac{2\cos\omega t}{1-\cos\theta}\right) \times \sin\omega t d(\omega t) + \frac{2V_o}{\pi}\int_{\pi-\beta}^{\pi}\sin\omega t d(\omega t) \tag{11}$$

$$= \frac{2V_o}{\pi}\frac{1-\cos\beta}{1+\cos\beta}\left(1+\cos\beta-\frac{\sin\beta^2}{1-\cos\beta}\right) + \frac{2V_O}{\pi}(1-\cos\beta) \tag{12}$$

$$= \frac{2V_o}{\pi}(1-\cos\beta). \tag{13}$$

Supposing the equivalent reactance of the rectifier with a capacitor filter and load resistance seen through $C_{fs}$ is $Z_{\rm eq}$, as shown in Fig. 3, which can be calculated as

$$Z_{\rm eq} = \frac{V_{C_{fs}}}{I_s} = \frac{\sin^2\beta}{\pi\omega C_{fs}} - j\frac{\pi-\beta+\sin\beta\cos\beta}{\pi\omega C_{fs}}. \tag{14}$$

Therefore, the equivalent resistance $R_{\rm eq}$ and equivalent capacitance $C_{\rm eq}$ are given by

$$\begin{cases} R_{\rm eq} = \frac{\sin^2\beta}{\pi\omega C_{fs}} \\ C_{\rm eq} = \frac{\pi C_{fs}}{\pi-\beta+\sin\beta\cos\beta}. \end{cases} \tag{15}$$

Using $Z_{\rm eq}$ to replace the rectifier with a back capacitor filter with load resistance, the equivalent circuit is shown in Fig. 4, where, $\boldsymbol{V_p}$, $\boldsymbol{I_p}$, $\boldsymbol{I_1}$, $\boldsymbol{V_s}$, and $\boldsymbol{I_s}$ are the phasors of the fundamental components of $v_p$, $i_p$, $i_1$, $v_s$, and $i_s$, respectively. Using KVL in loop circuit "1," we have

$$\frac{1}{j\omega C_{fp}}\boldsymbol{I_1} + j\omega L_{\rm fp}(\boldsymbol{I_1}-\boldsymbol{I_p}) = \boldsymbol{V_p}. \tag{16}$$

TABLE I
PARAMETERS OF EXPERIMENTAL PROTOTYPE

| Parameters | Values |
|---|---|
| $L_{fp}$, $L_p$, $M$, $L_s$ | 24.9 $\mu$H, 59.9 $\mu$H, 20.2 $\mu$H, 54.5 $\mu$H |
| $C_{fp}$, $C_p$, $C_s$, $C_{fs}$ | 149.4 nF, 40.2 nF, 64.4 nF, 64.4 nF |
| Switches of $Q_1$-$Q_4$, $D_5$-$D_8$ | IPP65R045, MBR20200 |

According to (16), as long as we design $\frac{1}{\omega C_{fp}} = \omega L_{fp}$, $|\boldsymbol{I_p}|$ would be a constant given as

$$|\boldsymbol{I_p}| = \frac{|\boldsymbol{V_p}|}{\omega L_{fp}}. \tag{17}$$

The constant $|\boldsymbol{I_p}|$ would induce a constant voltage $j\omega M\boldsymbol{I_p}$ in secondary side. Using KVL in loop circuit "3" of Fig. 4, we have

$$|\boldsymbol{I_s}| = \frac{M|\boldsymbol{V_p}|}{L_{fp}\sqrt{R_{\rm eq}^2+(\omega L_s-\frac{1}{\omega C_{\rm eq}})^2}}. \tag{18}$$

Without considering diode energy dissipation, the active energy consumed by $R_{\rm eq}$ equals to the energy consumed by $R_L$. Thus, we have

$$\left(\frac{|\boldsymbol{I_s}|}{\sqrt{2}}\right)^2 R_{\rm eq} = I_o^2 R_L. \tag{19}$$

Substituting (18) into (19), we can get

$$I_o = \frac{|\boldsymbol{V_p}|M}{\sqrt{2}L_{fp}}\frac{1}{\sqrt{R_{\rm eq}^2+(\omega L_s-\frac{1}{\omega C_{\rm eq}})^2}}\sqrt{\frac{R_{\rm eq}}{R_L}}. \tag{20}$$

According to the expressions of $R_{\rm eq}$, $C_{\rm eq}$, and $\beta$ in (3) and (15), we can learn that $I_o$ contains the parameter of $C_p$, $\omega$, $M$, $L_{fp}$, and $R_L$. In practice, we can select appropriate system parameters of $L_{fp}$ and $C_{fp}$ to quasi-CC output with small tolerance error.

For better comparison with the traditional FHA [5], [6], the output current $I_o$ under FHA is given by

$$I_o = \frac{2\sqrt{2}|\boldsymbol{V_p}|M}{\pi\omega L_{fp}L_s}. \tag{21}$$

It is clear that the output current $I_o$ is dependent of load resistance $R_L$ under traditional FHA, i.e., CC output can be achieved.

With the same designed parameters in the experimental part listed in Table I, the output current $I_o$ versus load resistance $R_L$ can be plotted, as shown in Fig. 5. It can be observed that not CC output but quasi-CC with appropriate 2 A can be achieved. The derivation error $\xi$ defined as $\xi = |I_o - I_N|/I_N$, which is smaller than 5% with load range of $R_L$ changing from 10 to 40 $\Omega$.

In practice, if traditional FHA is adopted to design LCC-P compensated IPT charger, the accuracy of charging current and charging speed would be deteriorated. To provide CC output with high accuracy to charge the battery, the proposed EFHA can be used to design LCC-P compensation network of IPT system based on the rated charging current and the variation range of equivalent resistance of battery. The design procedures of how to design the LCC-P compensated IPT system to achieve quasi-CC output are shown in Fig. 6. First of all, determine the

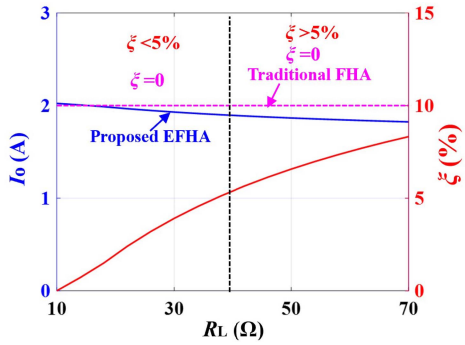


Fig. 5. Curves of $I_o$ and $\xi$ versus load resistance $R_L$.

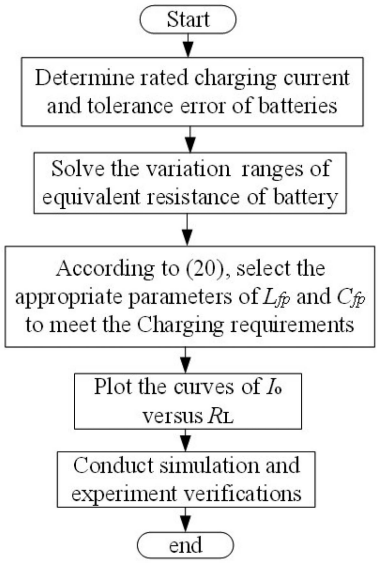


Fig. 6. Design procedures of achieving quasi-CC output.

rated charging current and tolerance errors of batteries. Next, the variation range of equivalent resistance of the batteries can be calculated based on the rated charging currents and voltages. Then, according to (20), we can design appropriate parameters of $C_p$, $M$, and $L_{fp}$ to satisfy the output requirements. Finally, do simulations and experiments to verify the accuracy of the designed LCC-P compensated battery charger. It should be noted that the proposed EFHA model can only be applied to static-induction-power-systems, where the relative position between the transmitting and receiving coils remains fixed during energy transfer.

## III. Simulation and Experimental Verifications

In order to verify the accuracy of the proposed EFHA of LCC-P compensated IPT converter, simulations and experiments are carried out under the parameters listed in Table I. The switching frequency is 85 kHz. Given a battery with capacity of 15 Ah, the desired constant charging current is set at $I_o = 2$ A.

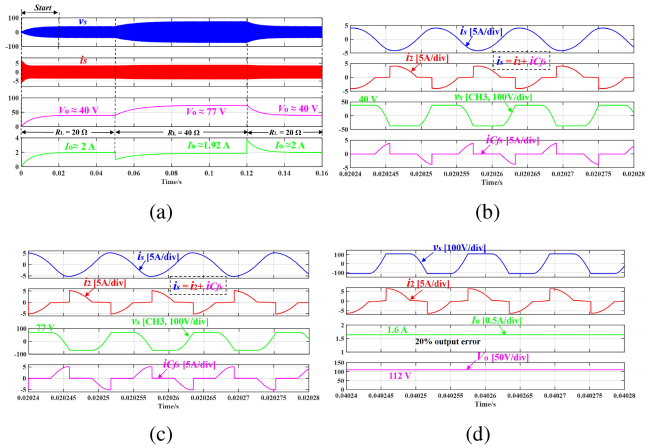


Fig. 7. Simulated results. (a) Transient waveforms under $R_L$ step changing from 20 to 40 Ω and back to 20 Ω. (b) Steady-state waveform with $R_L = 20\,\Omega$. (c) Steady-state waveform with $R_L = 40\,\Omega$. (d) Steady-state waveform with $R_L = 70\,\Omega$.

### A. Simulation Results

Fig. 7(a) shows the transient simulated waveforms of $v_s$, $i_s$, $V_o$, and $I_o$ under load step changing from 20 to 40 Ω and back to 20 Ω. It can be observed that quasi-CC output, i.e., $I_o \approx 2$ A, can be achieved, which is consistent with theoretical results shown in Fig. 5. Fig. 7(b) and (c) is the simulated steady-state waveforms of $i_s$, $i_s$, $v_s$, and $i_{C_{fs}}$ under $R_L = 20\,\Omega$ and $R_L = 40\,\Omega$, respectively. It can be observed that $i_2$ and $i_{C_{fs}}$ are discontinuous partial-sines waveforms while $i_s$ is a complete sine waveform. Moreover, the relationship between $i_2$ and $i_{C_{fs}}$ satisfies $i_s = i_2 + i_{C_{fs}}$, which have good agreements with theoretical waveform shown in Fig. 2. In addition, the simulated waveform of $v_{C_{fs}}$ is not an ideal square waveform which also shows good agreements with the theoretical analysis in Fig. 2.

Moreover, from Fig. 7(d), it can be observed that the output current $I_o$ would degrade significantly to 1.6 A with 20% error under $R_L = 70\,\Omega$ compared to the rated value of 2 A designed by traditional FHA calculation.

### B. Experimental Results

An overall experimental prototype is built, as shown in Fig. 8, to verify the accuracy of our proposed EFHA. The parameters are listed in Table I. The DSP TMS320F28335 is adopted as the microcontroller. An electronic load (PRODIGIT3302) is used to emulate the battery. All voltages and currents are recorded by a Tektronix DPO 4104 Oscilloscope. Powers, voltages, and efficiency values were measured by a precision power scope YOKOGAWA PX8000.

The experimental waveforms with the same simulated operating conditions of Fig. 6 are shown in Fig. 9. It can be observed that the experimental waveforms show good agreements with the simulation results shown in Fig. 7. These verifications confirm that only quasi-CC outputs can be achieved using LCC-P compensated IPT converters. Moreover, from Fig. 9(d), it can be

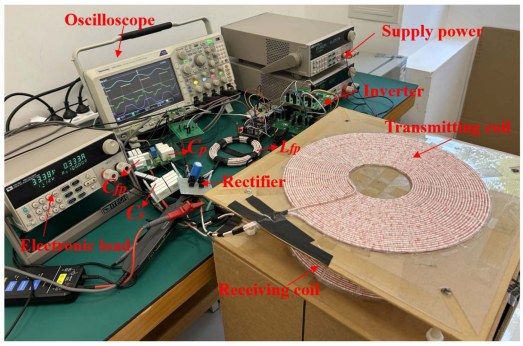


Fig. 8. Photo of experimental prototype.

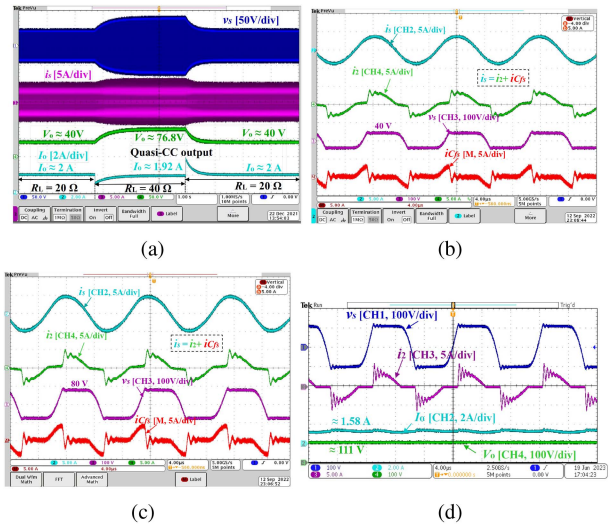


Fig. 9. Experimental results. (a) Transient waveforms under $R_L$ step changing from 20 to 40 Ω and back to 20 Ω. (b) Steady-state waveform with $R_L = 20\,\Omega$. (c) Steady-state waveform with $R_L = 40\,\Omega$. (d) Steady-state waveform with $R_L = 70\,\Omega$.

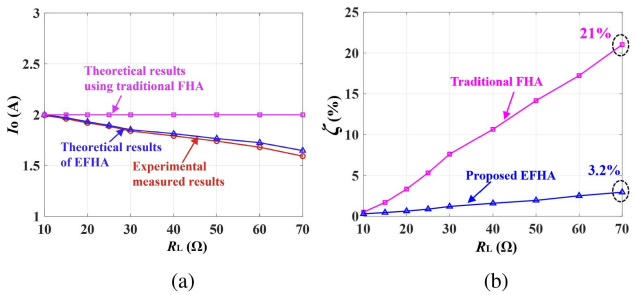


Fig. 10. Comparisons of measured results and output errors with theoretical FHA and EFHA. (a) Measured output currents. (b) Statistical errors.

observed that the measured output current $I_o$ would degrade significantly to 1.58. While, with our proposed EFHA, the derived output current model under $R_L = 70\,\Omega$ is 1.62 A, as shown in Fig. 10, which show good agreements and verify the accuracy of our proposed EFHA model. Compared with the simulated waveforms shown in Fig. 7, the experimental waveforms of $i_2$ and $i_{C_{fs}}$ have slight distortions, which are caused by parasitic inductance of the loop circuit.

Moreover, we also measure the output current $I_o$ versus load resistance $R_L$ in a wide range of variations. The measured output currents $I_o$ and corresponding calculated errors $\zeta$ are plotted in Fig. 10. The calculated output error $\zeta$ is defined as $\zeta = |\frac{\text{Measured I}_\text{o} - \text{Theoretical I}_\text{o}}{\text{Measured I}_\text{o}}| \times 100\%$. It can be observed that the quasi-CC output of 2 A with small error, e.g., $\zeta < 5\%$, can only be achieved when $R_L \leq 40\,\Omega$. With increase of the $R_L$, the output current $I_o$ would degrade significantly. The calculated output error $\zeta$ under our proposed EFHA are all less than 4%, which shows that our proposed EFHA is feasible and accurate. While, the values of $\zeta$ with traditional FHA would become larger with the increase of load resistance, and it will reach over 20% when $R_L$ is larger than $70\,\Omega$.

## IV. Conclusion

An EFHA of LCC-P compensated IPT system has been proposed in this letter, which can accurately derive the output current model of LCC-P compensated IPT converters. Both simulation and experiment results are both presented to validate the accuracy of EFHA. The results show that the output current would degrade with load resistance, and only quasi-CC output can be achieved in a certain load range. The proposed EFHA can be used to design the LCC-P compensated IPT system to achieve a quasi-CC output to satisfy the charging requirements, which has significant impacts on designing LCC-P compensated IPT charger practically.

## References

[1] X. Qu, H. Chu, S. Wong, and C. K. Tse, "An IPT battery charger with near unity power factor and load-independent constant output combating design constraints of input voltage and transformer parameters," *IEEE Trans. Power Electron.*, vol. 34, no. 8, pp. 7719–7727, Aug. 2019.

[2] Z. Huang, S. Wong, and C. K. Tse, "An inductive-power-transfer converter with high efficiency throughout battery-charging process," *IEEE Trans. Power Electron.*, vol. 34, no. 10, pp. 10245–10255, Oct. 2019.

[3] Y. Li et al., "Reconfigurable intermediate resonant circuit based WPT system with load-independent constant output current and voltage for charging battery," *IEEE Trans. Power Electron.*, vol. 34, no. 3, pp. 1988–1992, Mar. 2019.

[4] Z. Huang, G. Wang, J. Yu, and X. Qu, "A novel clamp coil assisted IPT battery charger with inherent CC-to-CV transition capability," *IEEE Trans. Power Electron.*, vol. 36, no. 8, pp. 8607–8611, Aug. 2021.

[5] Y. Gu, J. Wang, Z. Liang, and Z. Zhang, "Mutual-inductance-dynamic-predicted constant current control of LCC-P compensation network for drone wireless in-flight charging," *IEEE Trans. Ind. Electron.*, vol. 69, no. 12, pp. 12710–12719, Dec. 2022.

[6] Z. Yan, Y. Zhang, B. Song, K. Zhang, T. Kan, and C. Mi, "An LCC-P compensated wireless power transfer system with a constant current output and reduced receiver size," *Energies*, vol. 12, no. 1, pp. 1–14, Jan. 2019.

[7] A. Safaee and K. Woronowicz, "Time-domain analysis of voltage driven series–series compensated inductive power transfer topology," *IEEE Trans. Ind. Electron.*, vol. 32, no. 7, pp. 4981–5003, Jul. 2017.

[8] Y. Fang, B. M. H. Pong, and R. S. Y. Hui, "An enhanced multiple harmonics analysis method for wireless power transfer systems," *IEEE Trans. Ind. Electron.*, vol. 35, no. 2, pp. 1205–1216, Feb. 2020.

[9] J. Biela, U. Badstuebner, and J. W. Kolar, "Design of a 5-kW, 1-U, 10-kW/dm3 resonant DC–DC converter for telecom applications," *IEEE Trans. Power Electron.*, vol. 24, no. 7, pp. 1701–1710, Jul. 2009.